AIP Journal of Applied Physics

Broadband light trapping and absorption of thin-film silicon sandwiched by trapezoidal surface and silver grating

Wen-Bo Shi, Ren-Hao Fan, Kun Zhang, Di-Hu Xu, Xiang Xiong, Ru-Wen Peng, and Mu Wang

Citation: Journal of Applied Physics **117**, 065104 (2015); doi: 10.1063/1.4908006
View online: http://dx.doi.org/10.1063/1.4908006
View Table of Contents: http://scitation.aip.org/content/aip/journal/jap/117/6?ver=pdfcov
Published by the AIP Publishing

JOURNAL OF APPLIED PHYSICS 117, 065104 (2015)

Broadband light trapping and absorption of thin-film silicon sandwiched by trapezoidal surface and silver grating

Wen-Bo Shi, Ren-Hao Fan, Kun Zhang, Di-Hu Xu, Xiang Xiong, Ru-Wen Peng,[a)] and Mu Wang
National Laboratory of Solid State Microstructures and School of Physics, Collaborative Innovation Center of Advanced Microstructures, Nanjing University, Nanjing 210093, China

(Received 22 October 2014; accepted 31 January 2015; published online 11 February 2015)

In this work, we demonstrate the high optical absorption efficiency of a thin-film silicon solar cell. In thin-film solar cells, the efficiency is strongly dependent on light trapping by structures capable of exciting different resonance modes. Here, we consider a trapezoidal surface design that not only reduces reflection with a gradient index of refraction but also excites multiple cavity modes. The absorption can be enhanced further by combining a plasmonic structure, i.e., a silver grating. For comparison, we have separately simulated the silver grating structure, trapezoidal surface structure, and the combined structure. The combined structure retains all absorption effects shown by the individual components, achieving broadband absorption with a high efficiency. The investigations provide a unique design for high-performance solar cells of thin-film silicon. © *2015 AIP Publishing LLC*. [http://dx.doi.org/10.1063/1.4908006]

I. INTRODUCTION

Thin-film solar cells have aroused great interest in recent years because of their advantages in material cost and carrier collection. As we know, amorphous silicon (a-Si) films exhibit high electric defect density and low charge carrier diffusion length. However, electrical performances can be improved if a-Si solar cells are confined to a couple of hundreds of nanometers. Unfortunately, thin-film solar cell technologies are unavoidably limited by the absorption efficiency because of decreased absorption layer thickness.[1,2] To solve this problem, different nanostructures have been proposed to enhance the absorption of thin-film solar cells.[3] Antireflection nanostructures[4–11] are widely utilized to prevent light reflection. On the other hand, there have been numerous light-trapping structures (LTSs),[12–26] which can trap and couple light into the solar cell. For example, a reflector on the back of the solar cell can increase the path of light, and random metal particles can scatter the light into various directions in the solar cell. Plasmonic structures,[27–35] such as metallic core-shell nanoparticles using localized surface plasmons (LSP) and triangular metallic gratings using surface plasmon polaritons (SPP), have been applied widely in LTS to achieve high efficiency solar cells.

Recently, more and more studies have focused on broadband absorption in thin-film solar cells.[36–40] Usually, it is difficult to adopt one narrow-band effect to achieve high-efficiency light conversion. To solve this problem, various nanostructures, such as nanoparticles,[31] nanopillar arrays,[32] metal/dielectric gratings,[33] plasmonic fractal,[37] and nanowires[40] have been employed in the structured solar cells. In those systems, the combination of different resonance modes including SPP modes, LSP modes, and cavity modes significantly contributes to the broadband absorption. However, the efficiency of solar cell absorption can be improved further.

In this work, we design a thin-film silicon solar cell with conversion efficiency greatly enhanced through broadband absorption. In order to achieve this target, we have combined a gradient-index surface with a plasmonic structure. The designed solar cell is a periodic structure with a trapezoidal top surface and a metallic grating at the bottom of the absorber layer. Based on finite-difference time-domain (FDTD) method, we show theoretically that the light can be efficiently trapped in this solar cell as multiple resonance modes are excited. This particularly noticeable phenomenon occurs because of the trapezoidal surface, which provides an environment allowing the coexistence of multiple resonance modes, leading to broadband absorption and high efficiency.

II. STRUCTURE AND SIMULATION METHOD

Multiple modes are required for a broadband absorption. Here, we design a structure with a trapezoidal top surface and silver grating at the bottom of absorbing layer, as shown

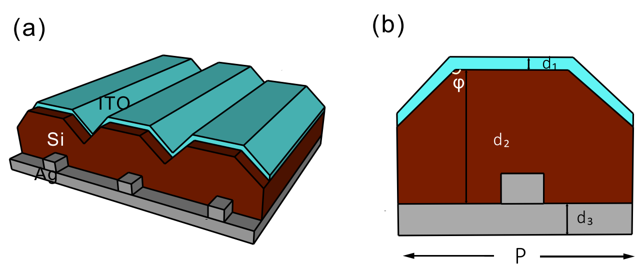

FIG. 1. The schematic (a) and (b) cross-sectional thin-film silicon solar cell with a trapezoidal top surface (vertex angle φ) and silver grating at the bottom. The three layers in this solar cell include an ITO layer (thickness d_1) on the top, an amorphous silicon absorbing layer (thickness d_2) in the middle, and a silver (Ag) layer (thickness d_3) on the bottom. The silver grating is embedded in the silicon layer at the silicon–silver layer interface.

[a)]Author to whom correspondence should be addressed. Electronic mail: rwpeng@nju.edu.cn in Figure 1.There are three layers: indium tin oxide (ITO) layer on the top, a-Si layer in the middle, and silver layer at the bottom. In our simulations, the optical constants of a-Si, silver, and ITO are with reference to the previous work.[41,42] The thicknesses from the top to bottom layers are $d_1 = 20$ nm, $d_2 = 210$ nm, and $d_3 = 80$ nm, respectively. We use d_2 to represent the thickest part of the silicon layer, and these thicknesses are unchanged in this work. With the trapezoidal top surface and silver grating at the bottom, more light can be trapped, leading to broadband absorption.

First, the trapezoidal surface supplies a gradient profile of the index of refraction because the effective index of refraction can be proportional to the volume fraction of the components. With this gradient profile, reflection of the incident light can be reduced. Moreover, different from conventional gradient index structure, the trapezoidal surface supplies a gradient profile not only for refractive index but also for the thickness of the silicon layer, the latter is the key factor for exciting multiple Febry-Perot (FP) resonances modes. FP modes can be excited when they satisfy a particular condition, which can be derived from the relationship between the wavelength with the refractive index n and thickness d, $\lambda_k \approx 2nd/k$,[43] where k is an integer that represents the order of FP resonance. With a gradient distribution of the thickness, different FP modes can be excited for large range of wavelengths, which explains why we can acquire broadband absorption with a comparably simple structure. The silver grating at the bottom is designed for SPP excitation. In fact, SPP modes arise via the coupling between light and electrons in the conductor, and they can be tailored by adjusting the structures on metal surface. The dispersion relation of SPP modes is given by[44] $k_{SP} = k_0\sqrt{\frac{\varepsilon_d \varepsilon_m}{\varepsilon_d + \varepsilon_m}}$, where k_{SP} is the wave vector of the surface plasmon, k_0 is the in-plane component of the incident wave vector, and ε_d and ε_m are permittivity of the dielectric and metal, respectively. According to the dispersion relation, momentum conservations are strictly required for SPP modes. The most common way to excite an SPP mode utilizes grating structures at the interfaces to satisfy the conservation of momentum.

We perform the numerical calculations using the FDTD method with Lumerical FDTD Solution 8.0.1. We consider transverse electric (TE) and transverse magnetic (TM) polarizations under *AM1.5G* solar radiation with normal incidence, using a single unit cell for periodic boundary conditions in the x-direction and perfectly matched layers (PMLs) boundary conditions in the y-direction. The mesh is set to 2.5 nm. In our simulation, the incident light wavelength is 400–900 nm. We set a 2D Frequency-domain field, and power detectors surround the solar cell to obtain the electric field intensity at each point.

III. NUMERICAL RESULTS AND DISCUSSIONS

A. Enhanced absorption of separated structures

As mentioned above, multiple resonance modes such as SPP and FP modes caused by the trapezoidal surface and silver grating are key factors in broadband absorption. For a simple investigation, we separately simulated the structure containing only the silver grating or trapezoidal surface, represented by S_1 and S_2, respectively. We also use S_3 to represent the designed solar cell. The absorption[45] of the solar cell at a given wavelength (λ) is evaluated by

$$A(\lambda) = \omega \cdot \mathrm{Im}(\varepsilon)\int |E|^2 dV, \tag{1}$$

where $Im(\varepsilon)$ is the imaginary part of the permittivity of silicon, ω and E are the angular frequency and the electric field, respectively, and the integral is over the silicon layer.

As shown in Figure 2(a), S_1 contains a silver grating with parameters of $d_1 = 20$ nm, $d_2 = 210$ nm, $d_3 = 80$ nm, $g = 50$ nm, $w = 100$ nm, $s = 135$ nm, and period $P = 370$ nm. Figure 2(b) shows the absorption spectrum of S_1 and a reference structure containing three bare layers of ITO, silicon, and silver. The red line shows TM polarization, the blue line shows TE polarization, and the dashed line shows the reference structure. It should be mentioned that the thickness of silicon in S_1 varies at different parts due to the silver grating. In both TE and TM polarization, the absorption is enhanced compared to the bare structure and the enhanced absorption appears mainly at long wavelengths around 800–900 nm. Then, we consider the effect of the trapezoidal surface on the absorption. As shown in Figure 2(c), S_2 contains a trapezoidal surface with three layers: ITO, silicon, and silver. The parameters are $h = c_1 = c_2 = 110$ nm and $P = 370$ nm. Figure 2(d) shows the absorption spectrum of S_2 and the reference structure. With the gradient thickness of silicon in S_2, anti-reflection and multiple FP modes are expected to enhance the absorption dramatically. Broadband absorption appears in S_2 compared to bare structure especially in TM polarization and the enhancement primarily occurs at short wavelengths from 400 nm to 700 nm. These two structures enhance the absorption in long and short wavelengths, respectively.

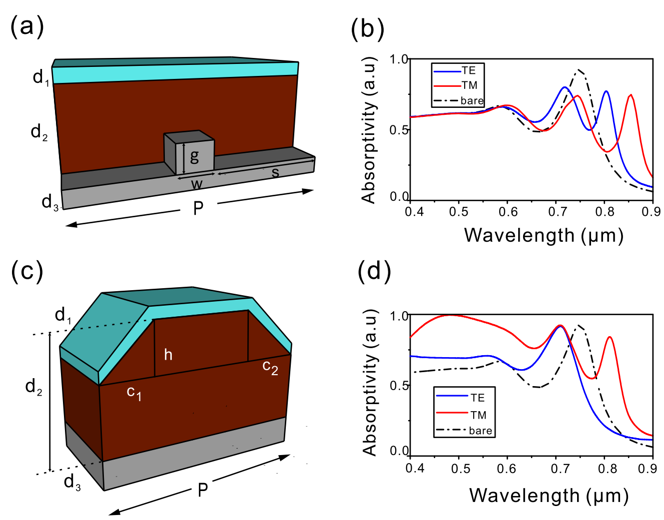

FIG. 2. (a) The S_1 structure with a silver grating at the bottom of the silicon layer. (b) Absorption spectrum of S_1, and a reference containing three bare layers of ITO, silicon, and silver. The enhancement occurs mainly in long wavelengths around 800–900 nm. (c) The S_2 structure contains the trapezoidal surface without the silver grating. (d) Absorption spectrum of S_2 and reference with vertically incident light. The enhancement occurs mainly in short wavelengths from 400 to 700 nm.

B. Broadband absorption of the combined structure

We have shown that the silver grating and trapezoidal surface improve absorption by different resonance modes and enhance the absorption for different parts of the whole spectrum. Thereafter, if we combine these two structures, multiple resonance modes are expected to excite in broadband, thus achieving broadband absorption. The combined structure S_3 is shown in Figure 3(a). The simulation was performed with the following parameters: $P = 370$ nm, $g = 50$ nm, $w = 100$ nm, $s = 135$ nm, and $h = c_1 = c_2 = 110$ nm. Figure 3(b) shows the absorption spectrum of S_3 in TE and TM polarization. The absorption enhancement at both short and long wavelengths indicates that by combining S_1 and S_2, multiple resonance modes are excited in S_3, thus broadband absorption can be acquired. But unfortunately, compared to the bare structure, the absorption of S_3 at the wavelengths from 700 to 800 nm decreases dramatically, which reduces the broadband effect. To find out the origin of absorption reduction, we have calculated the electric field distributions at $\lambda = 715$ nm in S_2 and S_3, respectively, because the absorption is strongly related to the electric field intensity (to see Eq. (1)). Figures 3(c)–3(f) clearly show that the presence of silver grating greatly influences the FP resonance modes in TE and TM polarization. Figure 3(f) shows that SPP mode appears at the interface of silver grating and silicon, while the FP mode that exists in S_2 disappears in S_3. In order to regain the absorption loss, we should revise our structure. We notice that the calculated S_1 and S_2 above are highly symmetrical structures, and their combination (S_3) is also symmetrical. The symmetry will play a negative role if we combine S_1 and S_2 directly, as shown in Figure 3. To improve our structure, the symmetry should be broken.

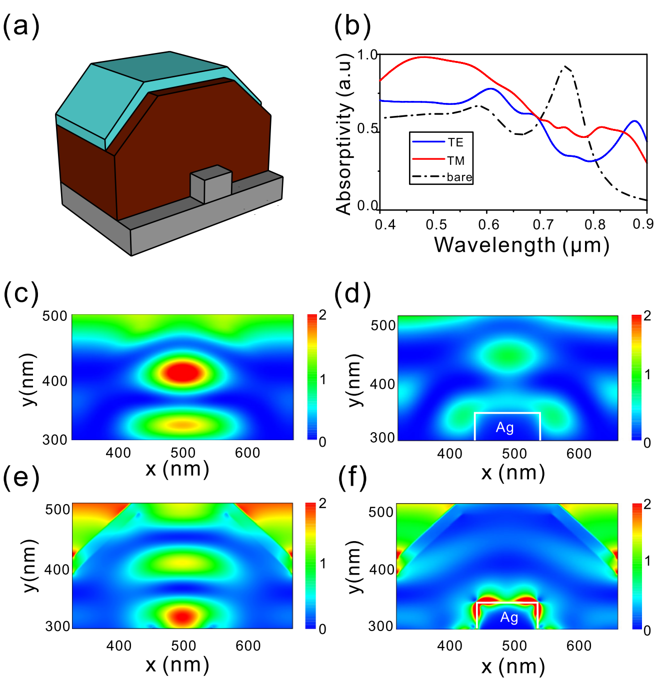

FIG. 3. (a) Combined structure S_3. (b) Absorption spectrum of S_3. Calculated electric field distributions: (c) $\lambda = 715$ nm, TE polarization in S_2 (d) $\lambda = 715$ nm, TE polarization in S_3. (e) $\lambda = 715$ nm, TM polarization in S_2. (f) $\lambda = 715$ nm, TM polarization in S_3. The presence of the silver grating obviously affects some of the FP resonance modes.

In order to regain the lost absorption caused by the symmetric structure, we modify the parameters to break the symmetry to improve the conversion efficiency. In the simulations, we have varied P from 370 to 490 nm, h from 90 to 165 nm, c_1 and c_2 from 110 to 145 nm, g from 40 to 90 nm, and s from 165 to 115 nm to get this optimized structure. Other parameters such as w, d_1, d_2, and d_3 are kept unchanged. As a result, we find the optimized parameters of S_3 to be $P = 430$ nm, $h = 160$ nm, $c_1 = 115$ nm, $c_2 = 140$ nm, $w = 100$ nm, $g = 80$ nm, and $s = 125$ nm. Figure 4(a) shows the absorption spectrum of the optimized S_3. Clearly, in the optimized S_3, broadband high absorption appears from 400 to 900 nm in both TE and TM. We get not only absorption enhancement at short wavelengths from 400 to 700 nm and long wavelengths from 800 to 900 nm but also regain the high absorption around 700–800 nm. Figure 4(b) shows the absorption spectrum of the optimized S_3 (marked as Op-S_3) and optimized S_2 (marked as Op-S_2) in TE and TM polarization. Actually, the optimized S_2 can be achieved by removing the silver grating from optimized S_3. The red line shows optimized S_3, and the blue dashed line shows optimized S_2. As we can see, the combined structure with the asymmetrical trapezoidal surface and silver grating performs much better than the structure containing only the asymmetrical trapezoidal surface in TE polarization and their performance is similar in TM polarization. With the broken symmetry of the modified structure, the additional silver grating greatly improves absorption in TE polarization due to more resonance modes and does not affect the absorption in TM very much. To prove the influence of the broken symmetry, we calculated the electric field distributions at $\lambda = 715$ nm in TE

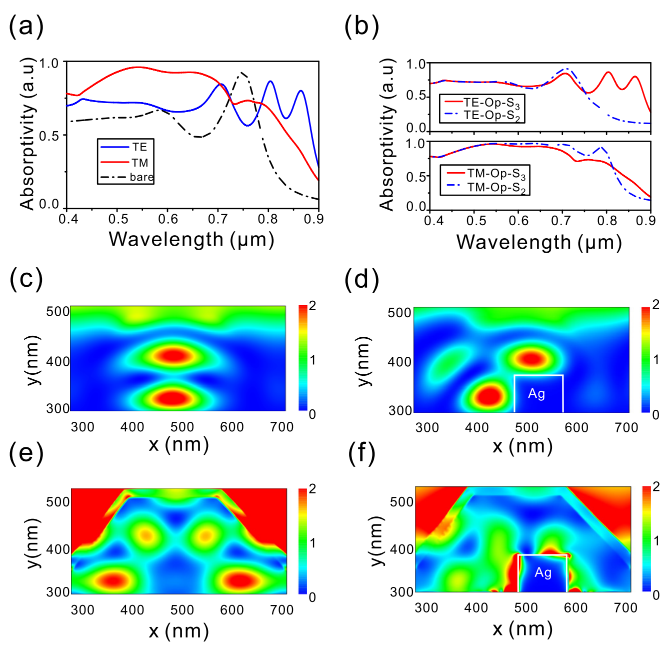

FIG. 4. (a) Absorption spectrum of the optimized S_3 structure. The blue line shows TE polarization, and the red line shows TM polarization. (b) Absorption spectrum of the optimized S_3 and S_2. Calculated electric field distributions: (c) $\lambda = 715$ nm in TE polarization of optimized S_2. (d) $\lambda = 715$ nm in TE polarization of optimized S_3. (e) $\lambda = 790$ nm in TM polarization of optimized S_2. (f) $\lambda = 790$ nm in TM polarization of optimized S_3. Compared with (c), (d) and (e), (f), the silver grating's influence on the FP resonance modes is very slight in the optimized S_3.

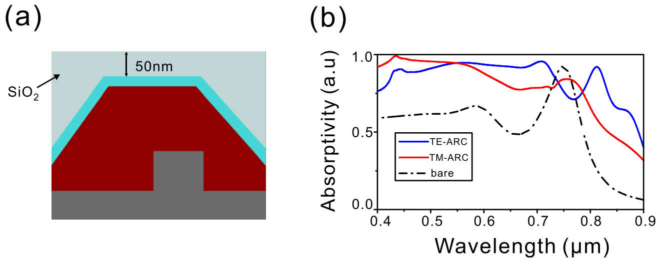

FIG. 5. (a)The optimized S_3 structure with SiO_2 ARC. The thinnest part of ARC is 50 nm. (b) Absorption spectrum of optimized S_3 with SiO_2 ARC. The red line shows TM polarization, and the blue line shows TE polarization. The absorption is enhanced over the whole range especially at short wavelengths.

polarization and $\lambda = 790$ nm in TM polarization for both S_2 and S_3, as shown in Figure 4. In TE polarization (Figures 4(c) and 4(d)), compared to symmetric structure shown in Figs. 3(c) and 3(d), FP resonance modes are preserved due to the broken symmetry and the absorption keeps equally strong as shown in Fig. 4(b). In TM polarization, for optimized S_2 in Figure 4(e), the electric field is strongly enhanced because of resonance mode. For optimized S_3 in Figure 4(f), although the FP mode is weaker than that in Fig. 4(e), we can still find it exist along with strong SPP mode, which is different from Fig. 3(f). As a result, by introducing the asymmetry, we have greatly improved the absorption.

C. Enhanced absorption by dielectric anti-reflecting coating (ARC)

Dielectric ARC is widely used in solar cells to reduce reflection. Here, we selected SiO_2 as the ARC material. As shown in Figure 5(a), we placed a SiO_2 film on top of the solar cell, which is 50 nm at its thinnest part. For general ARC film, anti-reflection occurs at a given wavelength dependent on the ARC thickness. Because we have a trapezoidal SiO_2 ARC film on the top, we have a gradient profile of thickness. By adding this ARC film, transmission of light can be enhanced in broadband range. Figure 5(b) shows the absorption spectrum of the optimized S_3 with ARC. The red line shows TM polarization, and the blue line shows TE polarization. Clearly, the absorption is enhanced over the whole band especially at short wavelengths. The effect of ARC is quite inspiring in TE polarization with highly enhanced absorption at short wavelengths. A broadband enhanced absorption is acquired by utilizing the ARC film.

We have also considered another two structures: one is to replace the silver with a perfect electronic conductor (PEC); and the other is to insert a 10 nm-thick ZnO layer between silicon and silver in optimized S_3 to explore the influence of SPP modes, as shown in Figs. 6(a) and 6(b). According to Figure 6(b), the absorption of silver decreases at the wavelengths 800–900 nm and in this range the absorption of silicon in PEC structure is weaker than that in optimized S_3 in TM polarization as shown in Fig. 6(a). This means that the absorption contribution from SPP modes mainly lies at long wavelengths from 800 to 900 nm. By utilizing the ZnO layer, the plasmonic losses are reduced as shown in Fig. 6(b). On the other hand, as shown in Fig. 6(a) the difference between PEC structure and optimized S_3 is small at short wavelengths, which indicates the absorption in this range is mainly from FP resonance modes deriving from front and backside nanostructure.

It is known that external quantum efficiency (*QE*) is defined as the ratio of the number of electrons in the external circuit produced by an incident photon of a given wavelength.[46] In this study, we consider an ideal process and assume that the recombination loss is zero and the carrier's lifetime is infinite when the solar cell is under 1 sun standard *AM1.5G* illumination, then the ideal *QE* can be given by[37]

$$QE = \frac{\int_{\lambda_1}^{\lambda_2} \frac{\lambda}{hc} A(\lambda) \times \mathrm{I}_{AM1.5G}(\lambda) d\lambda}{\int_{\lambda_1}^{\lambda_2} \frac{\lambda}{hc} \mathrm{I}_{AM1.5G}(\lambda) \mathrm{d}\lambda}, \tag{2}$$

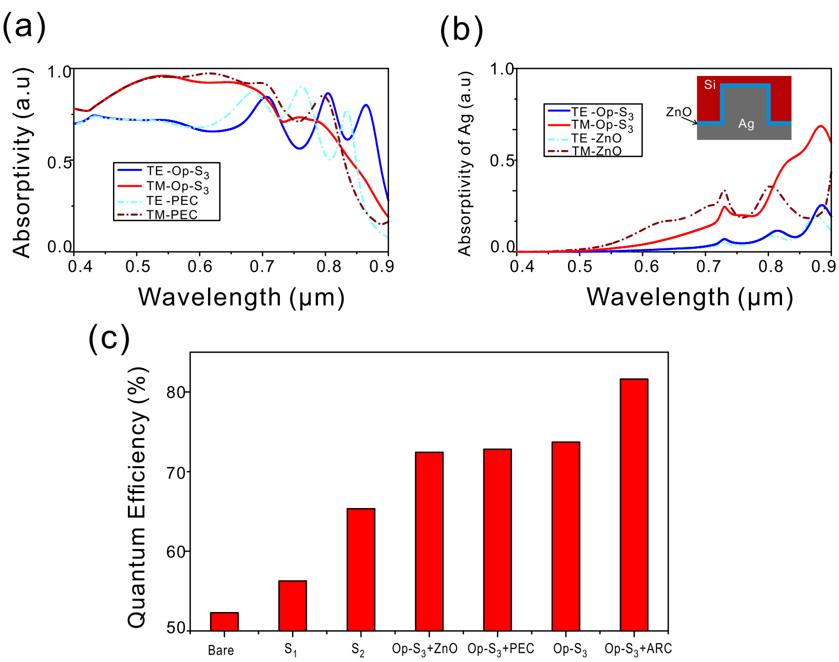

FIG. 6. (a) Absorption spectrum of optimized S_3 with PEC. (b) Absorption spectrum of Ag in optimized S_3 with ZnO layer. The inset shows the structure with ZnO layer. (c) Calculated quantum efficiencies of different structures with 210 nm-thick a-Si including the bare structure, S_1, S_2, optimized S_3 with ZnO, optimized S_3 with PEC, optimized S_3, and optimized S_3 with ARC. The respective *QEs* are 52.28%, 56.26%, 65.34%, 72.43%, 72.82%, 73.71%, and 81.62%. The absorption enhancement is 56.12% for the best condition.

where λ is the incident wavelength, h is Planck's constant, c is the speed of light in free space, $A(\lambda)$ is the average absorption of TE and TM polarizations, and $I_{AM1.5G}$ (λ) is the air mass 1.5 solar spectrum. The simulated wavelength range is from 400 nm to 900 nm.

We have calculated *QEs* of different structures with 210 nm-thick a-Si including the bare structure, S_1, S_2, optimized S_3 with ZnO, optimized S_3 with PEC, optimized S_3, and optimized S_3 with ARC, as shown in Figure 6(c). The absorption enhancement is defined as: $(QE\text{-}QE_b)/QE_b$, in which QE_b refers to QE of the bare structure. Under the best condition (optimized S_3 with ARC), the absorption enhancement is 56.12%. The *QEs* of optimized S_3 with ZnO, optimized S_3 with PEC, and optimized S_3 are very close, which show that the plasmonic losses are very limited in the proposed structure. On the other hand, the *QEs* remarkably increase when the silver grating and trapezoidal surface are introduced, demonstrating that light is more effectively trapped in our solar cell and converted to electric energy. As we have shown, broadband absorption due to multiple resonance modes is the key factor. The trapezoidal surface supplies a gradient profile of thickness, thus multiple modes are excited in broadband and the silver grating enhances this effect. The ARC film also plays an important role in improving the absorption. Therefore, with a trapezoidal surface, silver grating, and SiO_2 ARC, our solar cell acquires high *QE* due to broadband absorption.

IV. CONCLUSIONS

We have proposed a thin-film silicon solar cell with a trapezoidal top surface and a silver grating at the bottom of the silicon layer. Broadband absorption is acquired via the excitation of multiple resonance modes. The trapezoidal surface supplies a gradient profile of the refractive index as well as the thickness of silicon. Thus, the trapezoidal surface not only reduces reflection but also provides an environment allowing the coexistence of multiple resonance modes. The silver grating is designed to enhance absorption in long wavelengths, and we demonstrate that the silver grating improves the absorption when combined with the trapezoidal surface. By introducing the asymmetry, the absorption can be greatly enhanced. In this way, we achieve strong enhancement and high quantum efficiency due to broadband absorption.

ACKNOWLEDGMENTS

This work has been supported by the Ministry of Science and Technology of China (Grant Nos. 2012CB921502), the National Natural Science Foundation of China (Grant Nos. 11034005, 61475070, and 11474157).

[1]K. L. Chopra, P. D. Paulson, and V. Dutta, Prog. Photovoltaics **12**, 69 (2004).
[2]M. A. Green, J. Mater. Sci.: Mater. Electron. **18**, 15 (2007).
[3]H. A. Atwater and A. Polman, Nature Mater. **9**, 205 (2010).
[4]E. Yablonovitch and G. D. Cody, IEEE Trans. Electron Devices **29**, 300 (1982).
[5]H. W. Deckman, C. B. Roxlo, and E. Yablonovitch, Opt. Lett. **8**, 491 (1983).
[6]L. L. Ma, Y. C. Zhou, N. Jiang, X. Lu, J. Shao, W. Lu, J. Ge, X. M. Ding, and X. Y. Hou, Appl. Phys. Lett. **88**, 171907 (2006).
[7]Y. J. Lee, D. S. Ruby, D. W. Peters, B. B. McKenzie, and J. W. P. Hsu, Nano Lett. **8**, 1501 (2008).
[8]R. Dewan, M. Marinkovic, and R. Noriega, Opt. Express **17**, 23058 (2009).
[9]V. E. Ferry, M. A. Verschuuren, H. B. T. Li, E. Verhagen, R. J. Walters, R. E. I. Schropp, H. A. Atwater, and A. Polman, Opt. Express **18**, A237 (2010).
[10]C. A. Keasler and E. Bellotti, Appl. Phys. Lett. **99**, 091109 (2011).
[11]Y. C. Tsao, C. Fisker, and T. G. Pedersen, Opt. Express **22**, A651 (2014).
[12]C. Haase and H. Stiebig, Appl. Phys. Lett. **91**, 061116 (2007).
[13]A. Naqavi, K. Söderström, F. J. Haug, V. Paeder, T. Scharf, H. P. Herzig, and C. Ballif, Opt. Express **19**, 128 (2011).
[14]W. J. Nam, L. Ji, T. L. Benanti, V. V. Varadan, S. Wagner, Q. Wang, W. Nemeth, D. Neidich, and S. J. Fonash, Appl. Phys. Lett. **99**, 073113 (2011).
[15]D. Madzharov, R. Dewan, and D. Knipp, Opt. Express **19**, A95 (2011).
[16]R. Biswas and C. Xu, Opt. Express **19**, A664 (2011).
[17]U. W. Paetzold, E. Moulin, B. E. Pieters, R. Carius, and U. Rau, Opt. Express **19**, A1219 (2011).
[18]V. E. Ferry, A. Polman, and H. A. Atwater, ACS Nano **5**, 10055 (2011).
[19]J. Lacombe, O. Sergeev, K. Chakanga, K. von Maydell, and C. Agert, J. Appl. Phys. **110**, 023102 (2011).
[20]R. Dewan, J. I. Owen, D. Madzharov, V. Jovanov, J. Hüpkes, and D. Knipp, Appl. Phys. Lett. **101**, 103903 (2012).
[21]U. Palanchoke, V. Jovanov, H. Kurz, P. Obermeyer, H. Stiebig, and D. Knipp, Opt. Express **20**, 6340 (2012).
[22]S. Solntsev, O. Isabella, D. Caratelli, and M. Zeman, IEEE J. Photovoltaics **3**, 46 (2013).
[23]U. Palanchoke, V. Jovanov, H. Kurz, R. Dewan, P. Magnus, H. Stiebig, and D. Knipp, Appl. Phys. Lett. **102**, 083501 (2013).
[24]V. Jovanov, U. Planchoke, P. Magnus, H. Stiebig, and D. Knipp, Sol. Energy Mater. Sol. Cells **110**, 49 (2013).
[25]J. Eisenlohr, J. Benick, and M. Peters, Opt. Express **22**, A111 (2014).
[26]M. R. Khan, X. F. Wang, P. Bermel, and M. A. Alam, Opt. Express **22**, A973 (2014).
[27]S. A. Maier, P. G. Kik, H. A. Atwater, S. Meltzer, E. Harel, B. E. Koel, and A. A. G. Requicha, Nature Mater. **2**, 229 (2003).
[28]R. A. Pala, J. White, E. Barnard, J. Liu, and M. L. Brongersma, Adv. Mater. **21**, 3504 (2009).
[29]Y. H. Kuang, K. H. M. van der Werf, Z. S. Houweling, and R. E. I. Schropp, Appl. Phys. Lett. **98**, 113111 (2011).
[30]J. F. Zhu, M. Xue, H. J. Shen, Z. Wu, S. Kim, J. J. Ho, A. Hassani-Afshar, B. Q. Zeng, and K. L. Wang, Appl. Phys. Lett. **98**, 151110 (2011).
[31]Y. N. Zhang, Z. Ouyang, N. Stokes, B. H. Jia, Z. R. Shi, and M. Gu, Appl. Phys. Lett. **100**, 151101 (2012).
[32]H. P. Wang, K. T. Tsai, K. Y. Lai, T. C. Wei, Y. L. Wang, and J. H. He, Opt. Express **20**, A94 (2012).
[33]A. Abass, K. Q. Le, A. Alù, M. Burgelman, and B. Maes, Phys. Rev. B **85**, 115449 (2012).
[34]E. Battal, T. A. Yogurt, L. E. Aygun, and A. K. Okyay, Opt. Express **20**, 9458 (2012).
[35]M. Y. Lin, Y. L. Kang, Y. C. Chen, T. H. Tsai, and S. C. Lin, Opt. Express **22**, A438 (2014).
[36]W. Wang, S. M. Wu, K. Reinhardt, Y. L. Lu, and S. C. Chen, Nano Lett. **10**, 2012 (2010).
[37]L. H. Zhu, M. R. Shao, R. W. Peng, R. H. Fan, X. R. Huang, and M. Wang, Opt. Express **21**, A313 (2013).
[38]R. H. Fan, L. H. Zhu, and R. W. Peng, Phys. Rev. B **87**, 195444 (2013).
[39]W. Wang, Y. Hao, and Y. Cui, Opt. Express **22**, A376 (2014).
[40]K. D. Song, T. J. Kempa, H. G. Park, and S. K. Kim, Opt. Express **22**, A992 (2014).
[41]E. D. Palik, *Handbook of Optical Constants of Solids* (Academic Press, 1998), Vol. 3.
[42]D. Qu, F. Liu, Y. D. Huang, W. L. Xie, and Q. Xu, Opt. Express **19**, 24795 (2011).
[43]M. Yang, Z. P. Fu, F. Lin, and X. Zhu, Opt. Express **19**, A763 (2011).
[44]W. L. Barnes, A. Dereux, and T. W. Ebbesen, Nature **424**, 824 (2003).
[45]J. N. Munday and H. A. Atwater, Nano Lett. **11**, 2195 (2010).
[46]T. Markvart and L. Castaner, *Practical Handbook of Photovoltaics: Fundamentals and Applications* (Elsevier Advanced Technology, 2003), Chap. a1.